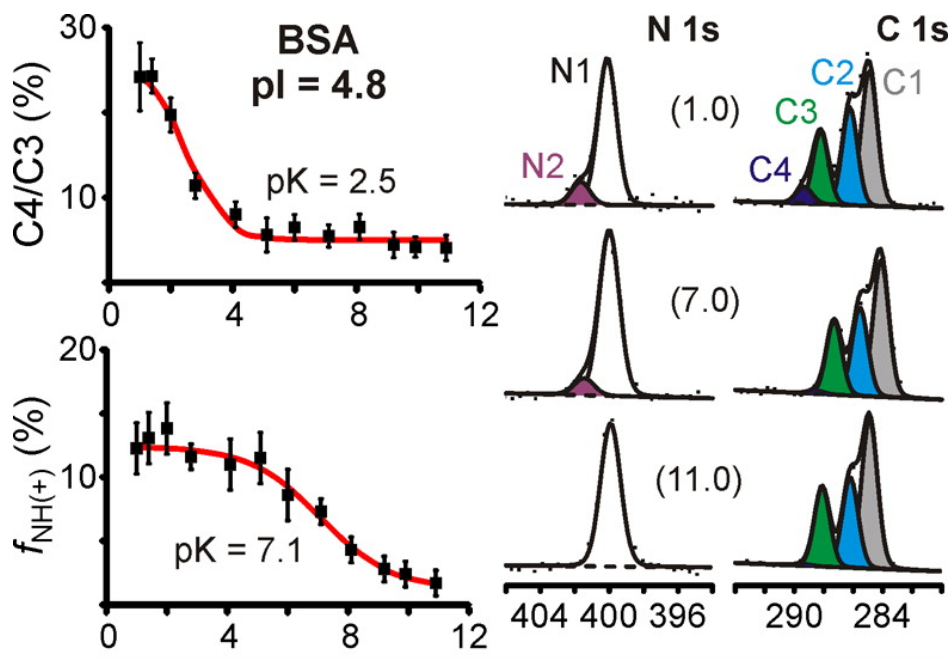


# Analytical Chemistry Cumulative Exam: X-ray Photoelectron Spectroscopy (XPS)

Prof. Luke Hanley, 9 May 2017

Please first read the attached paper: K.P. Fears, *Anal. Chem.* 86 (2014) 8526-9.

- (10%) Why did these experiments have to be performed on dried (rather than wet or hydrated) films of polypeptides and proteins?
- (15%) Explain this order of binding energies:  $C4 > C3 > C2 > C1$ , given the identified carbon atoms from which the photoelectron signal is emitted (see Figure 1 and caption).
- (20%) The X-ray photoelectron (XP) spectra shown in the paper are recorded using an Al- $K_{\alpha}$  monochromatic X-ray source. Give two reasons why these experiments would fail if a Mg- $K_{\alpha}$  achromatic X-ray source was used instead.
- (15%) The bottom spectrum in Figure 1 of cleaned Au shows a large C 1s contaminant peak in the XP spectrum. Why can contamination of the underlying Au substrate be ignored in these XPS analyses of relatively thick polypeptide and protein films? Your answer must consider the fundamental aspects of how XPS works.
- (15%) Why does the baseline signal often increase on the lower binding energy side of an XP peak? For example, see the N 1s peaks in the middle of Figure 2.
- (25%) The data in the attached paper for bovine serum albumin (BSA) in Figure 3 (shown below) was used to obtain a pI for BSA of 4.8 within the range of published values 4.5 – 4.9. Assume that a new paper declares BSA's pI to be definitively  $4.5 \pm 0.2$ . What experimental errors in the XPS measurement would you need to reconsider to reevaluate the 4.8 pI value? Recall that:  $pI = \frac{1}{2} (pK_1 + pK_2)$  and  $pH = pK + \log \left\{ \frac{[\text{conjugate base}]}{[\text{weak acid}]} \right\}$ .



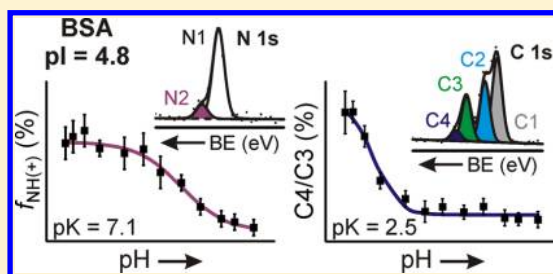
Measuring the  $pK/pI$  of Biomolecules Using X-ray Photoelectron Spectroscopy

Kenan P. Fears\*

Chemistry Division, Naval Research Laboratory, Washington, DC 20375, United States

## Supporting Information

**ABSTRACT:** Dissociation constants of GG–X–GG and  $X_5$  peptides (X = G, D, H, or K), and bovine albumin (BSA) and fibronectin (FN) were measured by X-ray photoelectron spectroscopy (XPS) in ultrahigh vacuum at room temperature. The biomolecules were deposited on Au substrates by drying 2.0  $\mu\text{L}$  drops of 1.0  $\mu\text{g } \mu\text{L}^{-1}$  stock solutions in 100 mM sodium phosphate buffers (pH 1–12) at room temperature. Because of the  $\sim+1.3$  eV shift in binding energy (BE) of protonated amines,  $pK$  values of basic amino acids were calculated by plotting the fraction of protonated amines as a function of solution pH. Similarly, the BE of carboxyl groups shifted  $\sim-1.3$  eV upon deprotonation. While C 1s spectra were convoluted by the multiple chemical states of carbon present in the samples, the ratio of the C 1s components centered at BE =  $289.0 \pm 0.4$  and BE =  $287.9 \pm 0.3$  proved to reliably assess deprotonation of carboxyl groups. The  $pK$  values for the Asp (3.1 and 2.4), His (6.7), and Lys (11.3 and 10.6) peptides, and the  $pI$  of BSA (4.8) and FN (5.7), were consistent with published values; thus, these methods could potentially be used to determine the dissociation constants of surface-bound biomolecules.



Because of the influence of electrostatic interactions on the folding, stability, solubility, and functionality of biomolecules, the importance of defining their acid/base dissociative properties has been recognized for nearly a century.<sup>1</sup> Without an understanding of these properties, discerning the mechanisms involved in biological processes would be extremely difficult, if not impossible. While potentiometric titration techniques and nuclear magnetic resonance (NMR) spectroscopy are commonly used for measuring the dissociation constants of ionizable moieties in solution, a wide range of other techniques have been reported in the literature, such as electrophoresis, UV–vis spectroscopy, circular dichroism, and chromatography.<sup>2–5</sup> Similarly, various techniques for measuring the dissociation constant of surface-bound moieties have been previously reported.<sup>6</sup> However, despite the high sensitivity of X-ray photoelectron spectroscopy (XPS) and the fact that ionized moieties exhibit distinguishable binding energy (BE) shifts from their neutral counterparts,<sup>7–9</sup> to date, no reports have detailed calculating the dissociation constants of biomolecules using XPS.

In recent *ex situ* XPS studies, we noted the observation of a secondary component corresponding to protonated amines in the N 1s spectra of surface-adsorbed peptides on various inorganic surfaces.<sup>10–12</sup> Despite thoroughly drying the samples and analyzing them under ultrahigh vacuum (UHV) at room temperature, the adsorbed peptides maintained their protonation states. This observation suggested that *ex situ* XPS could be used to determine the dissociation constants of biomolecules deposited on solid substrates by assessing their charge state as a function of the solution pH during deposition without the need

for techniques to keep biomolecules hydrated, such as freeze-drying, fast-freezing, or liquid microjets.<sup>13</sup>

The aim of this study was to establish and validate XPS methods for measuring the pH at which half the ionizable moieties present were protonated/deprotonated ( $pK$ ) and the isoelectric point ( $pI$ ) of biomolecules. Previous reports have shown that N 1s spectra of surface-adsorbed biomolecules can exhibit components shifted to lower BEs ( $\sim-1.3$  eV) than their main amide components if amide groups interact with the surface via contacts that involve significant charge transfer.<sup>10–12,14</sup> To avoid such interactions, thick biomolecular films were deposited on Au substrates from solutions ranging in pH from 1 to 12. GG–X–GG and  $X_5$  peptides, where “X” was Gly, Asp, His, or Lys, were analyzed to identify pH-dependent spectral changes related to the ionizable moieties. To evaluate their applicability to more complex systems, methods developed for the deposition and analysis of the model peptides were tested on bovine albumin (BSA, 66 kDa) and fibronectin (FN, 220 kDa).

## EXPERIMENTAL SECTION

**Sample Preparation.** All peptides used in this study were synthesized and purified (>98%) by GenScript USA Inc. with their N- and C-termini acetylated ( $-\text{COCH}_3$ ) and amidated ( $-\text{NH}_2$ ), respectively. BSA, FN, and all buffer reagents were used as received from Sigma-Aldrich Co. Stock solutions of the

Received: June 3, 2014

Accepted: August 5, 2014

Published: August 11, 2014

peptides and proteins ( $1.0 \mu\text{g} \mu\text{L}^{-1}$ ) were prepared in 100 mM sodium phosphate (pH 1–12) buffer solutions; pH was adjusted using NaOH and HCl.

Gold-coated silicon ( $\sim 100 \text{ nm Au}$ ) wafers from Platypus Technologies were used as substrates for XPS experiments. Prior to peptide and protein deposition, substrates were cleaned by sequential sonication in the following solutions for 5 min: 0.005% (v/v) Triton X-100, "piranha" wash [7:3  $\text{H}_2\text{SO}_4$  (98 wt %)/ $\text{H}_2\text{O}_2$  (30 wt %)], and "RCA standard clean 1" [1:1:5  $\text{NH}_4\text{OH}$  (28.0–30.0%  $\text{NH}_3$  basis)/ $\text{H}_2\text{O}_2$  (30 wt %)/ $\text{H}_2\text{O}$ ]. (Caution: Piranha solution is extremely oxidizing, reacts violently with organics, and should only be stored in loosely covered containers to avoid pressure buildup.) Substrates were rinsed with 18  $\text{M}\Omega \text{ cm H}_2\text{O}$  after each sonication step and dried under a stream of nitrogen gas at the completion of the cleaning process. Biomolecular films were formed by pipetting 2.0  $\mu\text{L}$  drops of stock solutions onto Au substrates and allowing them to dry at room temperature; regions absent of extensive crystallization were analyzed by XPS (Figure S1 in the Supporting Information).

**X-ray Photoelectron Spectroscopy.** XPS data were acquired at room temperature in an UHV analysis chamber with the base pressure  $< 5 \times 10^{-9}$  mbar. The spectrometer was equipped with a monochromated Al  $K\alpha$  X-ray source, the energy of which was calibrated and maintained at  $1486.6 \pm 0.2$  eV. The microfocussed X-ray source illuminated a spot of  $\sim 400 \times 600 \mu\text{m}^2$  on the substrate with a spatially uniform charge neutralization provided by beams of low-energy ( $\leq 10$  eV) electrons and  $\text{Ar}^+$  ions; charge neutralization device produced  $\sim 2 \times 10^{-7}$  mbar partial pressure of Ar in the analysis chamber during measurements. High-resolution spectra were acquired in the C 1s, N 1s, O 1s, and P 2p regions at a pass energy of 20 eV with 0.15 eV step size at a minimum of three separate spots for each sample (Note: sodium and chlorine are not shown but were present at varying amounts). The BE scale of the spectrometer was calibrated by an automated procedure to produce Au  $4f_{7/2}$ , Cu  $2p_{3/2}$ , and Ag  $3d_{5/2}$  peaks within 0.05 eV of standard reference values.<sup>15</sup>

XPS spectra were fitted in Unifit (ver. 2011), using a combination of Lorentzian and Gaussian line shapes to fit the individual components.<sup>16</sup> Backgrounds were modeled as part of the iterative fitting process using a linear combination of Shirley and linear functions. Multiple-component fittings were initiated with the lowest-BE component and its full-width at half-maximum (fwhm) was used to constrain the fwhm's for the other components. If the contribution of a fitted component fell below 1% of the individual spectrum, the component was omitted during the iteration process. Contributions to the fwhm from Lorentzian line shapes were fixed at 0.1 eV; Gaussian line shapes were allowed to vary between 1.2 and 1.3 eV (up to 1.4 eV for O 1s). Elemental compositions were quantified using calibrated analyzer transmission functions, Scofield sensitivity factors,<sup>17</sup> and effective attenuation lengths (EALs) for photoelectrons; EALs were calculated using the standard TPP-2M formalism.<sup>18,19</sup>

**Statistical Analysis.** Calculated values are reported as a mean plus or minus 95% confidence interval (C.I.) for  $n \geq 3$ .

## RESULTS AND DISCUSSION

Similar to our previous reports pertaining to peptides deposited on Au substrates,<sup>10,11</sup> adventitious contaminants detected on the clean substrates primarily consisted of aliphatic carbon (C1; Figure 1). Since glycine only has a single hydrogen atom in its

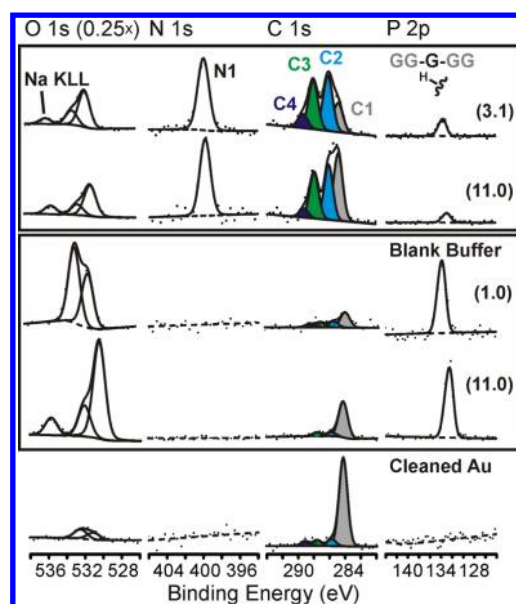


**Figure 1.** XPS spectra of the O 1s (0.25 $\times$  intensity), N 1s, C 1s, and P 2p regions collected from dried drops of GG–G–GG solutions, peptide-free buffers, and the cleaned Au substrate; numbers in parentheses indicate the solution pH. The N1 component corresponds to amide groups along the peptide backbone. The components in the C 1s spectra correspond to C–C groups (C1), C–O or C–N groups (C2), C=O groups (C3), and O–C=O or N–C=O groups (C4).

side chain, GG–G–GG was used as a nonionizable control. The N 1s spectra of GG–G–GG films deposited from acidic and basic solutions consisted of a single peak at BE  $\approx 400.0$  eV (Figure 1); thus, no nitrogen-containing groups were protonated. Also, the lack of a component in the N 1s region shifted to a lower BE indicated that there was no significant charge transfer between amide groups and the Au substrate within the analysis depth, contrary to a submonolayer of GG–G–GG adsorbed on Au.<sup>11</sup> Thus, monitoring the N 1s spectra presented a straightforward approach to assessing the percentage of protonated amines without interference.

Developing protocols to assess the degree of deprotonation among carboxyl groups was more convoluted than assessing the protonation of amine groups. Similar to the N 1s region, the BE of components related to carboxyl groups in the C 1s and O 1s regions are dependent on the protonation state.<sup>7–9</sup> However, as illustrated in Figure 1, the adsorption of atmospheric carbonaceous species is unavoidable and contributions to the O 1s region from phosphate ions vary with solution pH. While one could correct the O 1s spectrum of a peptide film based on the atomic percentage of phosphorus and the O 1s profile of the peptide-free buffer at the corresponding pH, these methods would be laborious and subject to error in the presence of additional charge species (i.e., ionizable amino acids) which could alter the dissociation of phosphate ions. Since the deprotonation of carboxyl groups result in BE shifts that are roughly equivalent to the difference between the C4 (O–C=O) and C3 (C=O) components, monitoring the C4/C3 ratio presented a simple alternative and adventitious carbon-containing species exhibited minimal contributions to these components (Figure 1).

For the His and Lys films, the N 1s spectra consisted of a main component (N1) at BE =  $400.0 \pm 0.2$  eV and a second component (N2;  $401.4 \pm 0.2$  eV) corresponding to protonated amines which was more pronounced at lower pHs (Figure 2).



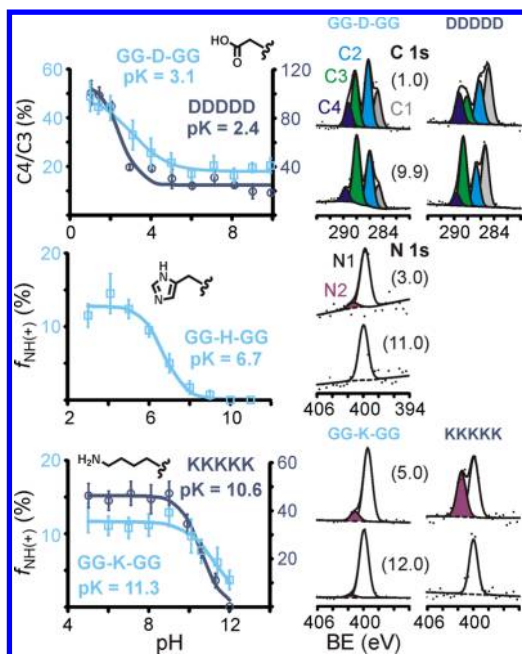


**Figure 2.** Normalized XPS spectra collected from Asp, His, and Lys films; numbers in parentheses indicate solution pH. Ratios of the C4 to C3 components and fraction of protonated amine groups (N2) are plotted as a function of solution pH. Plots were fit using eq 1 to determine pK.

The fractions of protonated amines were determined by peak fitting without further corrections. The maximum fraction of protonated amines were close to theoretical values based on peptide stoichiometry (Table 1), albeit GG–K–GG was significantly lower than its theoretical value. To determine the pK, the following equation was used to fit experimental data by minimizing the sum of the squared errors:

$$f = A \left[ \frac{10^{B(pK-pH)}}{1 + 10^{B(pK-pH)}} \right] + C \quad (1)$$

where  $A$  is the amplitude,  $B$  is related slope of the transition region,  $C$  is the minimum value, and pK is the pH at half-maximum. While a complete sigmoid curve is ideal, the pK values of the Lys peptides could be determined based on the assumption that  $C$  was equal to zero since the plots extended from the maximum ( $A$ ) through the half-maximum. The calculated pK values for the basic peptides (Table 1) were within the range of published pK values for His and Lys.<sup>20</sup>  $K_5$  exhibited a higher fraction of protonated amines and a pK value that was 0.7 pH units lower than GG–K–GG. The pK shift

was likely due to the electrostatic interactions between neighboring Lys residues in  $K_5$  increasing the local density of positive charges around the peptides.<sup>1</sup>

For the GG–G–GG films (Figure 1), the relative intensities of the components in the C 1s spectra were fairly consistent under acidic and basic conditions with the exception of the C1 component, which can be attributed to differences in adventitious contaminants adsorbing from the atmosphere. In contrast, the C4/C3 ratio in the C 1s spectra of the Asp films decreased with increasing pH (Figure 2). The use of this metric to measure pK was validated by agreement between the calculated pK value for GG–D–GG (3.1),  $D_5$  (2.4), and published values for Asp ( $3.5 \pm 1.2$ ).<sup>20</sup> Note that the assumption that fitting parameter  $C$  equals zero cannot be made for the Asp peptides; thus, determining both extremes of the curves were necessary. Like  $K_5$ , the pK value of  $D_5$  was shifted 0.7 units lower than its GG–X–GG counterpart. This was counterintuitive in that the multiple Asp residues should increase the local density of negative charges around the peptides, thus, shift the effective pK of  $D_5$  higher than GG–D–GG.<sup>1</sup> Because of Asp's short branched side chain, a possible explanation for the observed behavior is that the location of the carboxyl group with respect to the peptide backbone in  $D_5$  alters the polar environment surrounding the carboxyl groups, shifting the pK lower.

To evaluate the feasibility of using these protocols to measure the pK values of proteins, films of BSA and FN were prepared and analyzed in the same manner as the model peptides. Spectral shifts observed in the C 1s and N 1s regions of the proteins (Figure 3) were consistent with shifts in the spectra of the model peptides (Figure 2). BSA's theoretical maximum fraction of protonated amines agreed with the measured value (Table 1). Also, the calculated pI for BSA (4.8), the mean of its two pKs, is consistent with published values (4.5–4.9).<sup>21–23</sup> For FN, the maximum fraction of protonated amines obtained by XPS was nearly 5 times the theoretical value (Table 1), which reflects that the XPS sampling depth (3–10 nm) is smaller than the dimensions of FN molecules. However, the measured pI value (5.7) was near the range of pI values reported by van den Heuvel et al. (5.3–5.6),<sup>24</sup> indicating XPS is effectively sampling the entire surface of the FN molecules presumably due to the random orientation of the molecules in the films.

## CONCLUSIONS

The methods detailed in this study were validated by the agreement between measured pK/pI values and previously published values. Using the high sensitivity of XPS, these methods were capable of measuring the dissociation constants

**Table 1.** Maximum Percentage of Protonated Amines, pK, and pI Values for the Model Peptides and Proteins

	$f_{NH(+)} (%)$	$f_{NH(+)} (%)^a$	pK	pI	$pK^b$	pI
GG–D–GG			3.1		$3.5 \pm 1.2$	
DDDDD			2.4			
GG–H–GG	$12.7 \pm 1.4$	12.5	6.7		$6.6 \pm 1.0$	
GG–K–GG	$11.6 \pm 0.7$	14.3	11.3		$10.5 \pm 1.1$	
KKKKK	$46.4 \pm 1.9$	45.5	10.6			
BSA	$12.3 \pm 0.5$	12.8	2.5/7.1	4.8		4.5–4.9 <sup>c</sup>
FN	$20.7 \pm 0.8$	4.4	2.9/8.5	5.7		5.3–5.6 <sup>d</sup>

<sup>a</sup>Theoretical value based on stoichiometry (termini are acetylated or amidated). <sup>b</sup>Values reported in ref 20. <sup>c</sup>Values reported in refs 21–23. <sup>d</sup>Values reported in ref 24.

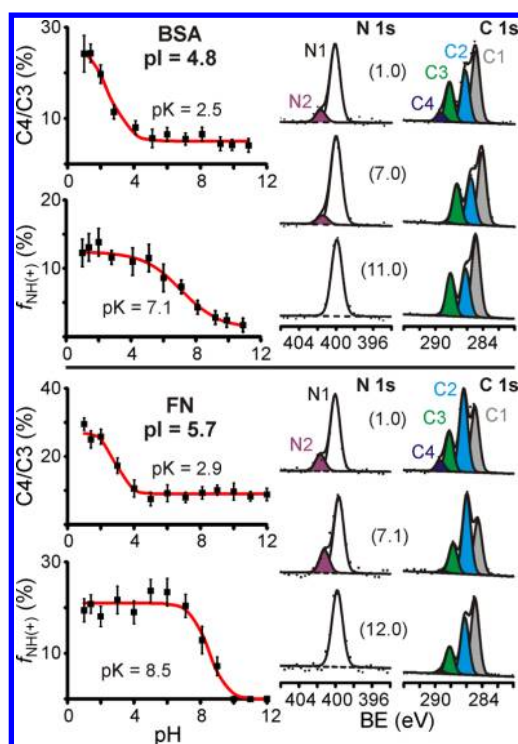


**Figure 3.** Normalized XPS spectra collected from BSA and FN films; numbers in parentheses indicate solution pH. Ratios of the C4 to C3 components and fraction of protonated amine groups (N2) are plotted as a function of solution pH. Data were fit using eq 1 to determine pK; pI was calculated as the mean value of the two pKs for each protein.

of biomolecules while requiring only micrograms of material. Since similar spectral shifts were observed for peptides at submonolayer surface densities,<sup>10–12</sup> these methods should be applicable at lower surface densities than used here. While these methods are not intended to supplant traditional techniques for measuring these properties in solution, they present a versatile approach for characterizing surface-bound biomolecules and other chemistries containing ionizable groups.

## ■ ASSOCIATED CONTENT

### 📄 Supporting Information

Image captured from K-alpha spectrometer of a dried GG–K–GG film on an Au substrate. This material is available free of charge via the Internet at <http://pubs.acs.org>.

## ■ AUTHOR INFORMATION

### Corresponding Author

\*E-mail: [kenan.fears@nrl.navy.mil](mailto:kenan.fears@nrl.navy.mil).

### Notes

The author declares no competing financial interest.

## ■ ACKNOWLEDGMENTS

This work was supported by the Office of Naval Research (ONR) through the basic research program at NRL.

## ■ REFERENCES

- (1) Pace, C. N.; Grimsley, G. R.; Scholtz, J. M. *J. Biol. Chem.* **2009**, *284*, 13285–13289.
- (2) Andrew, C. D.; Warwicker, J.; Jones, G. R.; Doig, A. J. *Biochemistry* **2002**, *41*, 1897–1905.
- (3) Slampova, A.; Krivankova, L.; Gebauer, P.; Bocek, P. *J. Chromatogr., A* **2009**, *1216*, 3637–3641.

- (4) Asenstorfer, R. E.; Jones, G. P. *Tetrahedron* **2007**, *63*, 4788–4792.
- (5) Seclaman, E.; Sallo, A.; Elenes, F.; Crasmareanu, C.; Wikete, C.; Timofei, S.; Simon, Z. *Dyes Pigm.* **2002**, *55*, 69–77.
- (6) Fears, K. P.; Creager, S. E.; Latour, R. A. *Langmuir* **2008**, *24*, 837–843.
- (7) Brown, M. A.; Vila, F.; Sterrer, M.; Thurmer, S.; Winter, B.; Ammann, M.; Rehr, J. J.; van Bokhoven, J. A. *J. Phys. Chem. Lett.* **2012**, *3*, 1754–1759.
- (8) Immaraporn, B.; Ye, P.; Gellman, A. J. *J. Phys. Chem. B* **2004**, *108*, 3504–3511.
- (9) Parker, B.; Immaraporn, B.; Gellman, A. J. *Langmuir* **2001**, *17*, 6638–6646.
- (10) Fears, K. P.; Petrovykh, D. Y.; Clark, T. D. *Biointerphases* **2013**, *8*, 1–20.
- (11) Fears, K. P.; Clark, T. D.; Petrovykh, D. Y. *J. Am. Chem. Soc.* **2013**, *135*, 15040–15052.
- (12) Fears, K. P.; Petrovykh, D. Y.; Photiadis, S. J.; Clark, T. D. *Langmuir* **2013**, *29*, 10095–10101.
- (13) Shchukarev, A. *Adv. Colloid Interface Sci.* **2006**, *122*, 149–157.
- (14) Petrovykh, D. Y.; Kimura-Suda, H.; Whitman, L. J.; Tarlov, M. J. *J. Am. Chem. Soc.* **2003**, *125*, 5219–5226.
- (15) Seah, M. P.; Gilmore, L. S.; Beamson, G. *Surf. Interface Anal.* **1998**, *26*, 642–649.
- (16) Hesse, R.; Streubel, P.; Szargan, R. *Surf. Interface Anal.* **2007**, *39*, 381–391.
- (17) Scofield, J. H. *J. Electron Spectrosc. Relat. Phenom.* **1976**, *8*, 129–137.
- (18) Jablonski, A.; Powell, C. J. *Surf. Sci. Rep.* **2002**, *47*, 35–91.
- (19) Tanuma, S.; Powell, C. J.; Penn, D. R. *Surf. Interface Anal.* **1994**, *21*, 165–176.
- (20) Grimsley, G. R.; Scholtz, J. M.; Pace, C. N. *Protein Sci.* **2009**, *18*, 247–251.
- (21) Salgin, S.; Salgin, U.; Bahadir, S. *Int. J. Electrochem. Sci.* **2012**, *7*, 12404–12414.
- (22) Yan, J.; Du, Y.-Z.; Chen, F.-Y.; You, J.; Yuan, H.; Hu, F.-Q. *Mol. Pharmaceutics* **2013**, *10*, 2568–2577.
- (23) Ran, D.; Wang, Y.; Jia, X.; Nie, C. *Anal. Chim. Acta* **2012**, *723*, 45–53.
- (24) van den Heuvel, M. J.; Jefferson, B. J.; Jacobs, R. M. *J. Virol.* **2005**, *79*, 8164–8170.